ISSN 1998-0124 CN 11-5974/O4
https://doi.org/10.26599/NR.2026.94908535

Research Article

Prediction and inverse design for ultrafast laser colorization on aluminum via color-morphology coupled neural network

Xianghong Xu[1,§], Jiaqun Li[2,3,§], Junjie Li[4], Haoze Han[2,3], Rui Han[2,3], Weiqing Li[1](✉), Zhaoyuan Ma[4], Yuichi Kozawa[5], Jianfeng Yan[2,3](✉)

[1] School of Engineering and Technology, China University of Geosciences (Beijing), Beijing 100083, China

[2] Department of Mechanical Engineering, Tsinghua University, Beijing 100084, China

[3] State Key Laboratory of Tribology in Advanced Equipment, Tsinghua University, Beijing 100084, China

[4] School of Automation and Intelligent Manufacturing, Southern University of Science and Technology, Shenzhen 518055, China

[5] Institute of Multidisciplinary Research for Advanced Materials, Tohoku University, 2-1-1 Katahira, Aoba-Ku, Sendai 980-8577, Japan

[§] Xianghong Xu and Jiaqun Li contributed equally to this work.

Nano Res., **Just Accepted Manuscript** • https://doi.org/10.26599/NR.2026.94908535
https://www.sciopen.com/journal/1998-0124 on Feb. 3, 2026

Just Accepted

Research Article

Prediction and inverse design for ultrafast laser colorization on aluminum via color-morphology coupled neural network

Xianghong Xu[1,§], Jiaqun Li[2,3,§], Junjie Li[4], Haoze Han[2,3], Rui Han[2,3], Weiqing Li[1,], Zhaoyuan Ma[4], Yuichi Kozawa[5], and Jianfeng Yan[2,3,*]*

[1]School of Engineering and Technology, China University of Geosciences (Beijing), Beijing 100083, China

[2]Department of Mechanical Engineering, Tsinghua University, Beijing 100084, China

[3]State Key Laboratory of Tribology in Advanced Equipment, Tsinghua University, Beijing 100084, China

[4]School of Automation and Intelligent Manufacturing, Southern University of Science and Technology, Shenzhen 518055, China

[5]Institute of Multidisciplinary Research for Advanced Materials, Tohoku University, 2-1-1 Katahira, Aoba-Ku, Sendai 980-8577, Japan

[§]Xianghong Xu and Jiaqun Li contributed equally to this work.

Received: 6 January 2026; **Revised:** 1 February 2026; **Accepted:** 3 February 2026

Address correspondence to Weiqing Li, liweiqing@cugb.edu.cn; Jianfeng Yan, yanjianfeng@tsinghua.edu.cn

Cite this article: *Nano Research*, **2026**, *19*, 94908535. https://doi.org/10.26599/NR.2026.94908535

Abstract:

Laser surface colorization has been regarded as a promise technology for inkless printing due to its advantages such as versatile, stable and environmentally friendly. However, the further applications of laser colorization in real industrial manufacturing are limited by inevitable trial and error procedure in experiment. Here, a prediction and inverse design of laser surface colorization process are realized to address this challenge by using a Color-Morphology Coupled Neural Network (CMCNN). The forward prediction is conducted by a Physical-guided Multilayer Perceptron (PG-MLP) with improved prediction accuracy. For solving the non-uniqueness of inverse design procedure, a Convolution Neural Network (CNN) based on the input physical image is utilized. This enables the combining of structural color and morphology information in input physical image for processing parameters planning. The network performance is verified through the fabrication of portrait and artwork image. The corresponding relationship between target color and experimental results demonstrate the validity of proposed model. This approach may open new possibilities

for the fast and precise surface colorization, and facilitate the development of laser structure fabrications in practical engineering applications.

Keywords: ultrafast laser, laser colorization, prediction and inverse design, neural network

1. Introduction

Structural color has received great attention as a promising technology for inkless printing and special marking owing to its advantages[1-3]. In contrast to conventional pigment or dyes, structural color behaves more long-term stable and environmentally friendly[4,5]. There have been several mechanisms and approaches for generating structural color, including photonic crystals[6], meta-surfaces[7,8], coating structures[9], and plasmonic effect[10]. For instance, a 3D-printed photonic crystals were fabricated by heat-shrinking method, which can realize sub-100-nm features with a full range of colors[11]. A meta-surface relying on polarization control was produced to control light propagation and realized encoding and decoding pseudo-color nano-printing images[12].

Recently, laser direct writing method have been found rather appreciate for surface structure fabrication for its facile processing procedure and large-scale machining abilities[13-15]. Laser induced structural color also holds higher stability and convenience compared to aforementioned techniques. Ultrafast laser in particular, is remarkable for its capacity to fabricate varieties of materials and micro /nano surface structures[16-19]. It is reported that efficient colorization of metal surfaces can be achieved with low power ultrafast lasers by temporally and spatially controlled laser scanning, allowing a wide spectrum of colors[20,21]. Most study on ultrafast laser induced structural color only investigate the unidirectional experimental relationship between laser parameters and final structural color[22-24]. It means that only those experimental verified color can be produced with corresponding laser processing situations[25]. However, for real manufacturing and further engineering applications, it is necessary to achieve efficient structure fabrication even if the corresponding relationship is unknown. Therefore, the prediction of ultrafast laser processing results and inverse parameter design without redundant experiments become much more important.

With the development and applications of artificial intelligence, there have been some works which can realize the approximate prediction of fabrication results and parameters through deep learning[26-28]. It is demonstrated that machine learning (ML) can help predict the spectra and colors of laser-induced structure and optimize the laser processing[29]. An artificial neural network combined with Response Surface Methodology (RSM) based experimental design can give the influence of the processing parameter on color changes of titanium[30]. To further explore the connection between structural colorization and processing conditions, some inverse design approaches are proposed, which are enabled by advanced deep neural network (DNN) like generative adversarial networks (GAN) and physical-informed neural networks (PINN)[31-33]. Through trained inverse models, laser processing parameters can be determined and optimized to fabricate target structural colorization[34,35]. Nonetheless, laser colorization is a complicated fabrication procedure involving multiple physical and chemical processes, including ablation, oxidation, melting and re-solidification[36]. Introducing physical priors into the training of neural networks has been shown to markedly enhance the ability of tandem neural network (TNN) models to predict laser processing parameters and the resultant coloration of processed metal surfaces. Given the complex mechanisms involved in laser processing and the still incomplete understanding of the underlying physics, efficient and accurate inverse design of processing parameters for large-area metal surfaces using neural-network-based learning and inference remains a challenging task.

Currently, most inverse-design studies use color alone as the input to predict processing parameters while neglecting the surface morphology of the structures, which fail to handle the one-to-many mapping scenarios. In fact, ultrafast laser processing parameters and scanning settings affect not only the color of the processed surface but also its textural morphology, which is an important consideration in surface design and color characterization. Convolutional neural network models can learn both color and texture features from images, and thus hold promise for structural-color design of large-area patterns, which is suitable to realize one to one generation of laser processing parameters from imported information.

In this work, we demonstrate the forward and inverse design of ultrafast laser structural colorization with a Color-Morphology Coupled Neural Network Model (CMCNN). The CMCNN model is composed of a Physical-guided Multilayer Perceptron (PG-MLP) for forward prediction and an Image-based convolutional neural network (CNN) for inverse design. By introducing beam overlap ratio (BOR) and average deposited energy (ADE) as extra physical factors, the prediction accuracy of forward MLP network can be efficiently raised. With the help of physical image information, the trained CNN we used called Efficient Net can achieve laser processing parameter approximation including repetition rate, pulse energy, scanning space and speed. Using the CMCNN model, multitype structural color on aluminum film can be inversed designed and experimentally validated. Furthermore, the Maxwell portrait and an artwork painting are fabricated with our proposed method. This work provides an alternative for precise structural color surface manufacturing and exhibit potentials for information storage and encryption applications.

2. Results and discussion

In traditional forward prediction model, only initial parameters are considered as input factors of training network. Although the prediction accuracy can be promoted via the optimization of loss function, the nonlinear and indirect complicated relationship between processing results and laser scanning settings retards the improvement of model. In real laser manufacturing, some factors which can be calculated by initial parameters are more related to the physical process, which may contribute to the final structure formation. These calculated derived parameters have a more direct relationship with final structure formation compared to initial parameters. The final structure formation is determined by initial parameters, and these derived parameters cannot solely determine the final structure formation. As shown in **Figure 1a**, two extra parameters including overlap ratio and average power are considered as inputs of forward network. The physical-guided MLP model is trained to predict the structural color on aluminum surface. For the inverse design of laser fabrication procedure, an image-based Efficient Net is utilized to obtain corresponding processing parameters, including repetition rate, scanning speed, scanning space and pulse energy. To solve the one-to-many problem, the textual morphology information is collected as another input of the CNN model. The total Model combining the forward MLP and inverse CNN is named Color-morphology Coupled Neural Network with the induction of physical calculated parameters and physical textural images. **Figure 1b** demonstrates the scanning process of femtosecond laser direct writing on the aluminum film surface. The repetition rate and scanning speed are considered and set together to obtain an adequate overlap ratio of the wind scanning route. A femtosecond laser fabricated colorization aluminum surface is displayed in **Figure 1c**. The scanning speed varies from 100 to 900 $mm \cdot s^{-1}$ and the pulse energy ranges from 36.78 to 79.22 J/cm^2, while maintaining a fixed scanning space and repetition rate. With the scanning speed and pulse energy increasing, the structural color gradually changes from yellow to navy blue, which is characterized and shown in **Figure 1d**. Structural color is extracted from optical images as the input data of PGNN for further training. Each optical image is photographed from the same view angle to ensure the consistence of color characterization. To gain a better demonstration of the structural colors which can be achieved, **Figure 1e** displays the CIE 1931 chromaticity diagram with several typical measured colors plotted in the sRGB triangle area. The result is found to cover most of the visible light color (the sRGB area) range from red to blue which means it can realize surface colorization with a wide color gamut. Using the fabricated structural color, an inkless patterned picture of the Auditorium in Tsinghua can be processed as shown in **Figure 1f**. It can be observed that the building composed of yellow, black and white is surrounded by trees composed of yellow and black, which is controlled with specific laser processing parameters.

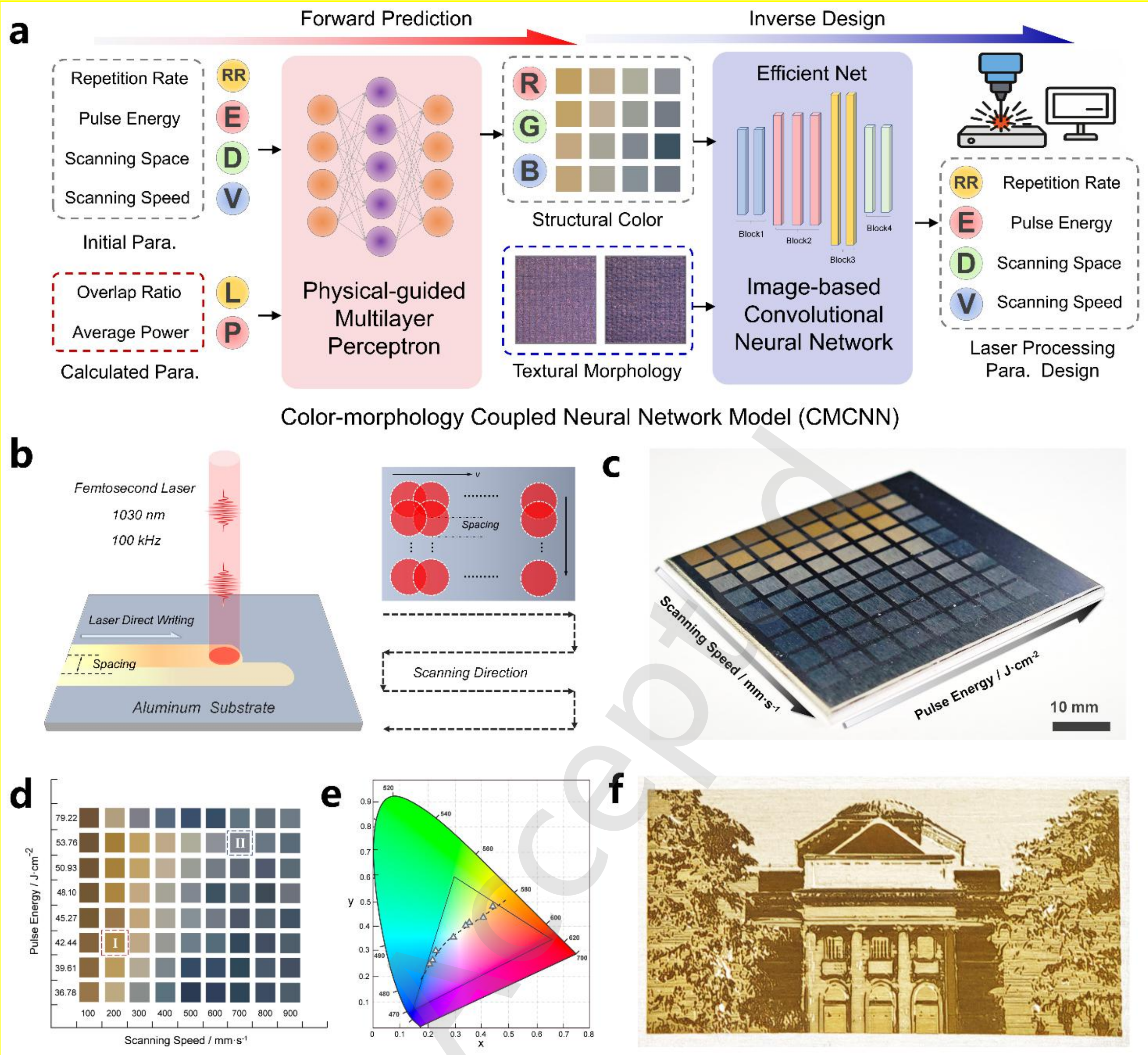

Figure 1. Schematic of Prediction and Inverse Design for Ultrafast Laser Colorization on Aluminum via a CMCNN Model composed of Physical-guided Multilayer Perceptron and Convolutional Neural Network. a, The CMCNN Model which can realize the forward prediction of structural color with a Physical-guided MLP and achieve the inverse design of laser processing parameters through an Image-based CNN. **b,** Schematics showing how the femtosecond laser realize the direct writing procedure. **c,** Different structural color fabricated on Al film with varied laser scanning speed and single pulse energy. **d,** Obtained Structural color display with scanning speed of 100-900mm·s^{-1} and pulse energy of 36.78-79.22 J/cm^2. **e,** Display of experimental measured structural color in CIE 1931 chromaticity diagram, the triangle area represents the sRGB area. **f,** The inkless patterned picture of the Auditorium in Tsinghua with femtosecond laser on a 30×60mm Al film.

To realize the results prediction and parameters design, the forward prediction and inverse-design model are discussed. The forward prediction model PGMLP is displayed in **Figure 2a**, which is based on a multilayer perceptron architecture. The initial inputs of model contain laser parameters and scanning settings including laser repetition, single pulse energy, laser scanning space and scanning speed. The performance of forward prediction model with initial inputs only is limited for the influence of initial parameters is indirect.

In real laser manufacturing process, some comprehensive factors are more related to the final machining results. Compared to considering the repetition rate and scanning speed individually, the ratio of repetition rate to scanning speed, which defines the scanning overlap, is more important to laser fabrication than either parameter alone. This is because the beam overlap ratio may govern the ablation and oxidation behavior during laser processing. Subsequent pulses at the same position will cause further ablation processes, which eventually determine both the surface structure and the resultant oxidation. That is, the degree to which the beam is overlapped at the same position more directly determines the resultant structure. Moreover, the average power, given by the product of pulse energy and repetition rate, plays an important role in the laser energy depositing procedure and influences the structure evolution. As the calculated factors are more crucial for the physical process than the initial parameters, the BOR and ADE parameters are introduced into the input of model as physical-driven parameters. Combining the initial and physical-driven parameters, the inputs of model are imported into a multilayer perceptron framework. The MLP framework consists of six layers while each layer is composed by a Fully Connected Layer and a Rectified Linear Unit. The size of Fully Connected Layer in the first layer is (6,512) and the others are (512,512). A Fully Connected Layer of (512,3) size is inserted between the Multilayer Perceptron and the final output to realize the RGB values prediction. The experimental dataset is shown in **Figure 2b**, which is composed by hundreds of data points obtained from laser fabrication experiment on an aluminum surface. Each data point contains four experimental parameters including laser repetition, single pulse energy, laser scanning speed represented in a coordinate system and scanning space represented by different colors. The scanning speed ranges from 100 to 500 mm/s while the scanning space varies from 1 to 11 μm. The repetition frequency of laser ranges from 1 to 200 kHz while the pulse energy varies from 15 to 30 J/cm^2. The overlap ratio and average power can also be calculated based on initial parameters and are imported into the prediction model.

The dataset of prediction model is randomly divided into a training dataset (900 sets of data) and a test dataset (226 sets of data). The output RGB values of prediction model is characterized and plotted in a CIE 1931 chromaticity diagram demonstrated in **Figure 2c**. It can be observed that the final structural color is evenly distributed and covers above 25% of the sRGB area. **Figure 2d** displays the correlation heat map between six input parameters and output structural colors RGB values. All the input and output parameters are found to show strong linear correlations with themselves, and have no obvious linear correlations with other indicators. It is meant that there is a lack of significant linear correlation between these parameters and no need to worry about low learning efficiency originated high redundancy. The scatter plots of training data and test data are shown in **Figure 2e**. It can be found that most of the data are located near the function y = x (gray dot lines), indicating that the predicted RGB values are well matched with the actual colors. The average Pearson correlation coefficients of training network is 0.91, which exhibit a notable correlation while 0.9222 for the red, 0.9156 for the green, and 0.8908 for the blue. The comparison of training results between original MLP model and Physical-guided MLP is displayed in **Tabel S1**, where an obvious promotion of Pearson correlation coefficients can be found.

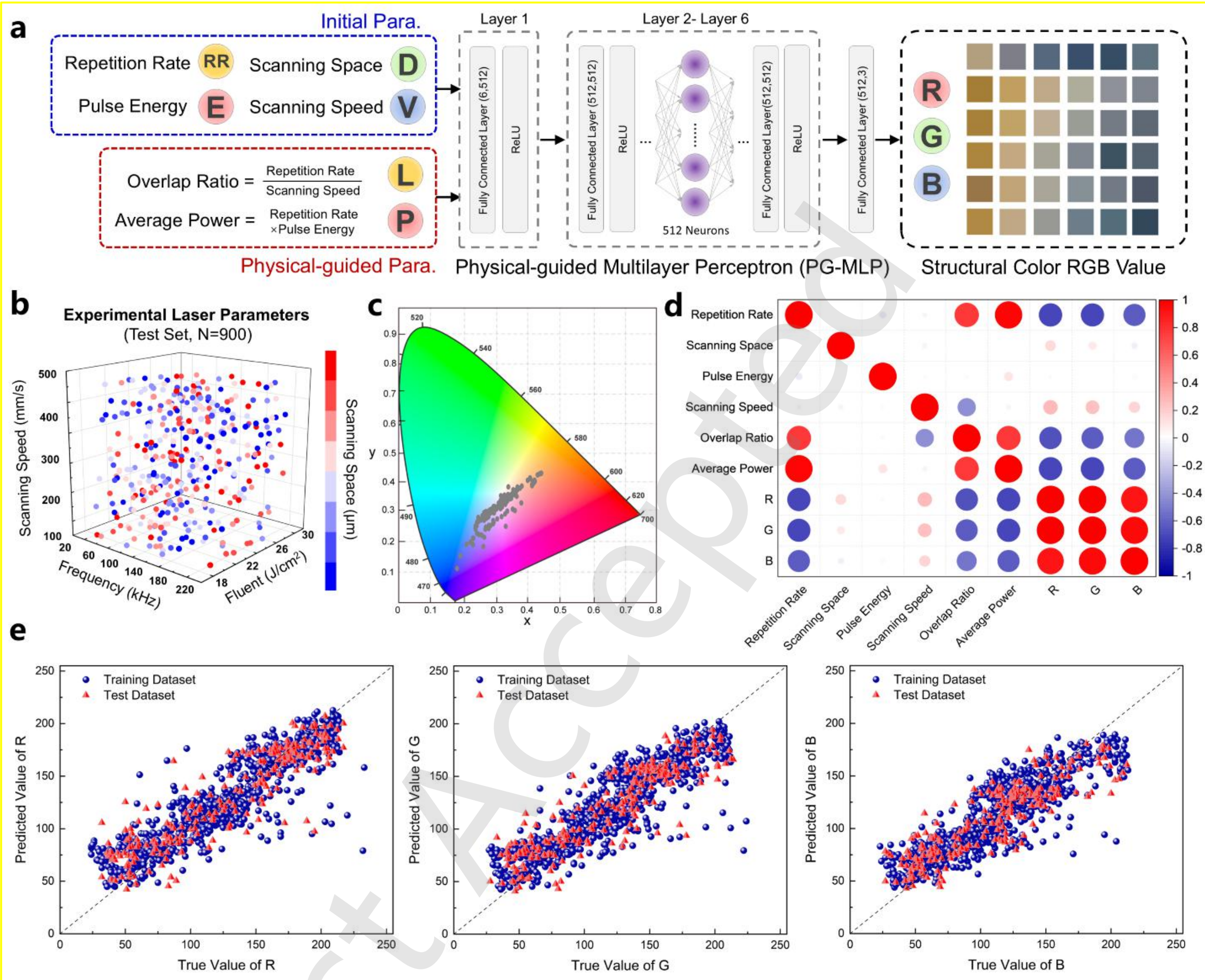

Figure 2. Forward prediction of laser fabricated structural color with PG-MLP model and details of training dataset. a, Schematic of the physical-guided multilayer perceptron model. The input contains initial parameters and calculated physical driven parameters. **b,** Distribution of training and test data with different experiment laser parameters. **c,** The CIE 1931 chromaticity diagram for structural color characterization of part of the training dataset. **d,** Correlation heat map between input parameters and output structural colors. **e,** Scatter plots for the demonstration of the difference between predicted value and true value of structural color, the gray dot lines represent the function y=x.

To obtain the laser processing parameters for the target structural color in real manufacturing, a convolution neural network combined target color and physical morphology image is demonstrated in **Figure 3a**. The main architecture of inverse design model is an Efficient Net consisted of nine stages. The input of the network is a picture of 224×224 pixel image which contains the structural color information and the surface textural morphology information. Through a normal convolutional layer with a kernel size of 3×3 and a stride of 2 in stage 1, the size of input image can be converted into 112×112 resolution. MBConv structures are repeated and stacked in stage2 to stage8 with different layers (1,1,2,2,3,3,4,1 layer as the diagram displays), which consists of two normal Convolution layers for dimensional upward and reduction, a $k \times k$ (k=3 or 5) Depthwise Convolution layer, a Squeeze & Excitation module and a Dropout layer. The final Stage 9, containing a normal 1×1 convolution layer, an average pooling layer and a fully connected layer, is connected with a regression head to output the corresponding processing parameter values based on the classified data.

The dataset of inverse network is the same as prediction model, and the color information and textural morphology information obtained from structure images are added into training. Based on the efficient network, the inversed-designed laser processing parameters can be obtained according to the given target structural information. As shown in **Figure 3b**, three target structural colors with corresponding experiment result based on obtained parameters are plotted on the CIE 1931 chromaticity diagram. It is observed that the location of experiment results almost coincides with the target values, which confirms the performance of the inverse design model. The detailed information of target structure and experimental result with designed parameters is displayed in the illustration on the upper right. It can be found that there is good agreement between the input target image and the experimental result derived from the inverse-designed parameters. The loss curve of training and validation for the inverse design model is demonstrated in **Figure 3c**. After 80-100 training epochs, the loss function of the inverse model can be reduced to a low value. **Figure 3d** shows the scatter plots of inverse design model train results, which indicates the difference between the inverse-deigned parameters and real values of the test dataset. The average Pearson correlation coefficients is 0.73 while the Pearson correlation coefficients of each parameter are 0.8279 for repetition rate, 0.6134 for scanning space and 0.7224 for overlap ratio. For the remaining parameters, Pearson correlation coefficients are given in the supplementary materials.

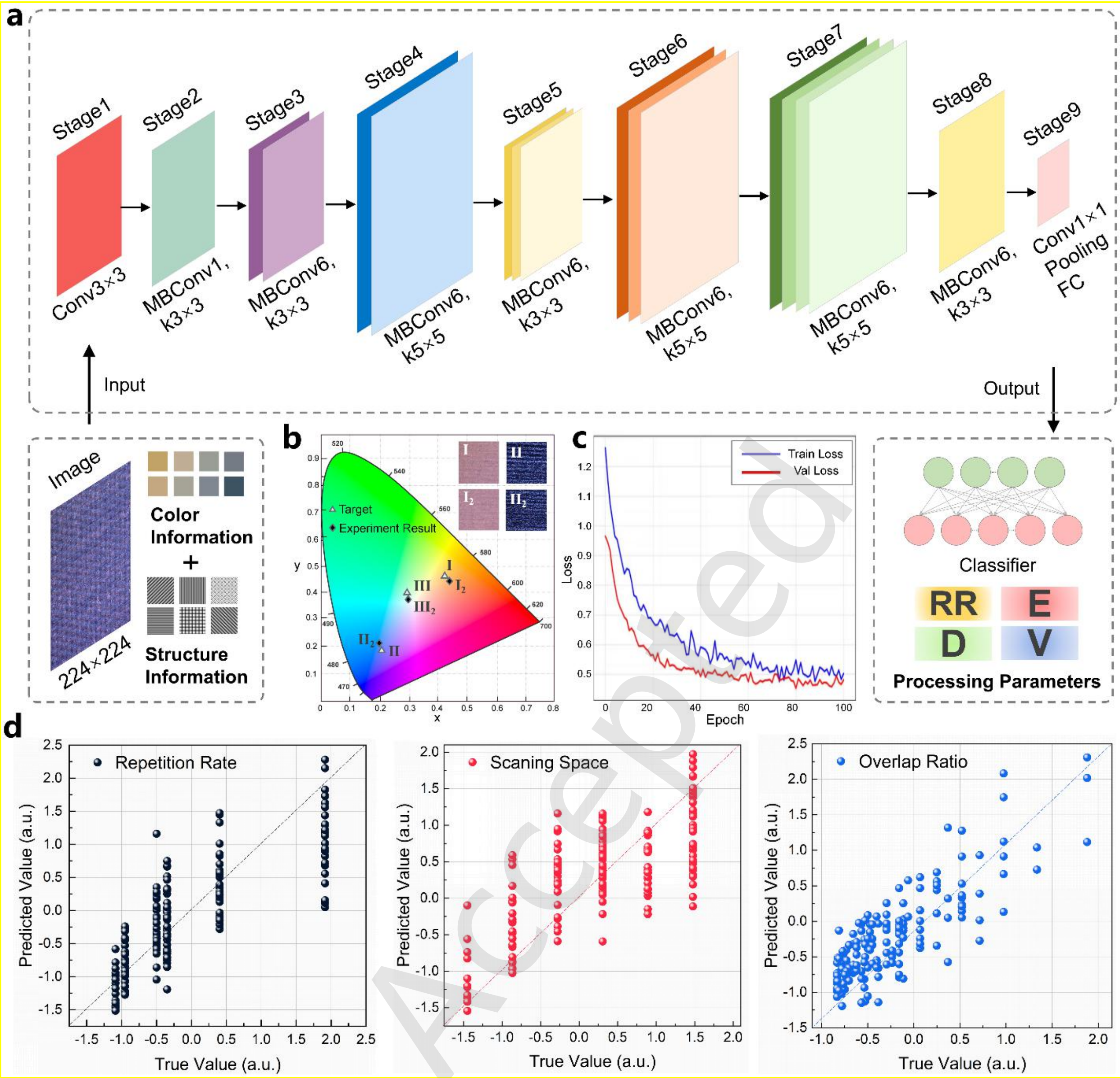

Figure 3. Inverse design of laser processing parameters for given structural color and structure. a, Architecture of the inverse design framework used to generate processing parameters based on the provided input information. **b,** Target structural color and corresponding experiment results based on the inverse design network plotted on the CIE 1931 chromaticity diagram. **c,** Loss curve of inverse design model with the epochs of training increasing. **d,** Scatter plots for the demonstration of difference between the inverse-deigned parameters and the real values of the test dataset.

To validate the feasibility of proposed Color-morphology Coupled Neural Network Model, the laser fabrication experiments are conducted and the results are illustrated in **Figure 4**. As shown in **Figure 4a** and **4b**, a Chinese article named ʻYue yang Tower Inscriptionʼ and a portrait for Maxwell are processed with two or three different colors designed by Physics-guided Neural Network Model, with structure morphology optical images displayed in illustrations. The experimental colors have a great match with the target value. To further evaluate the inkless colorful printing capacity, an artwork image fabricated with multiple colors is displayed in **Figure 4c**. The artwork image is composed of the moon in white, the lake in blue, the mountains in black and the buildings in yellow, which has clear and defined edges.

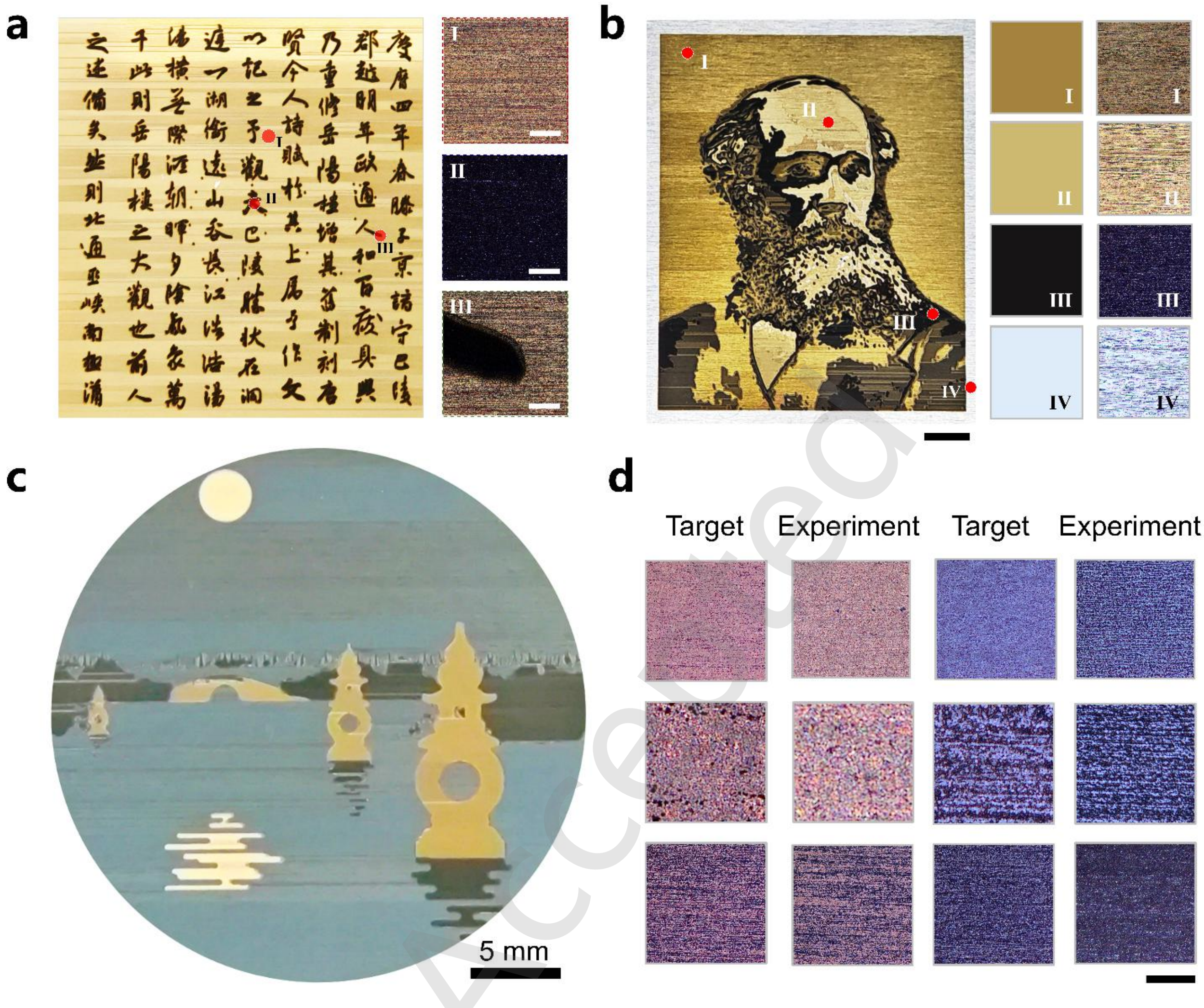

Figure 4. Characterization of laser fabricated structural color samples and validation for the inverse design model. a, Sample of an article in Chinese printed on an aluminum film surface, the illustrations on the right are the optical photographed images of different areas, the scale bar in illustration is 50μm. **b,** Sample of a portrait for Maxwell, the scale bar in illustration is 5 mm, the illustrations on the right are the RGB color obtained from different colored areas. **c,** Laser fabricated sample of an artwork image. **d,** Comparison of other target structural color and real fabricated result, the scale bar in illustration is 50 μm.

Figure 4d presents the comparison between the target value and real experiment result of other typical colors. The target structure image is imported into the inverse design model and the corresponding laser processing parameters are generated and calculated, including repetition rate, scanning speed, scanning space and pulse energy. Using the inverse-designed parameters, the real structure and color of validation experiment results are shown next to the imported images. As displayed in **Table 1**, the processing parameters were inverse-designed based on both target RGB values and structural information. Real colors were fabricated by using these parameters. The RGB values of real experimental colors were extracted from the optical photographed images, which have a good match relationship with target RGB values. The laser fabricated structural color samples and validation experiment indicate that the Color-morphology information Coupled Neural Network provides an efficient and feasible alternative to realize the prediction and design for laser colorization on metal surface, exhibiting adequate practicality in industrial and engineering applications.

Table 1. The comparison of target colors and real experimental results with inverse-designed processing parameters.

Target Color							
Real Color							
Target RGB	*192,129,149*	*175,139,151*	*160,124,157*	*105,104,173*	*120,116,170*	*61,56,121*	*65,59,105*
Real RGB	*189,134,147*	*195,155,167*	*158,119,148*	*103,112,173*	*126,123,183*	*31,56,112*	*63,63,110*
Repetition Rate	*43.5 kHz*	*37.3 kHz*	*72.6 kHz*	*87.0 kHz*	*2 kHz*	*32.8 kHz*	*94.4 kHz*
Scanning Speed	*163 mm/s*	*200 mm/s*	*500 mm/s*	*450 mm/s*	*12 mm/s*	*148 mm/s*	*175 mm/s*
Scanning Space	*7.1 μm*	*5.8 μm*	*5.7 μm*	*1.4 μm*	*0.5 μm*	*0.9 μm*	*4.4 μm*
Pulse Energy	*21.14 J/cm^2*	*22.38 J/cm^2*	*22.38 J/cm^2*	*19.89 J/cm^2*	*19.89 J/cm^2*	*21.14 J/cm^2*	*23.62 J/cm^2*

3. Conclusions

In conclusion, a Color-morphology Coupled Neural Network is proposed to achieve prediction and inverse design of laser structural colorization on metal surface. Using a Physical-guided Multilayer Perceptron model, the predicted structural color RGB values can be obtained with given laser processing parameters. The structural color obtained by this method can cover at least 25% of the sRGB region in the CIE 1931 chromaticity diagram. To solve one-many problems in the inverse design of laser parameters from target color information, a Convolution Neural Network combining imported structural color and morphology information is utilized to generate the corresponding laser fabrication conditions. The average Pearson correlation coefficients of forward and inverse model are above 0.91 and 0.73. The structural colorized samples with the comparison between target and experimental results confirm the feasibility and practicality of the coupled neural network. The current model and method focused on femtosecond laser processing and one specific material. The approach will be applied to various materials, additional laser parameters, and other types of lasers. This model and method offer a facile and efficient approach to realize laser machining design and surface structure processing, which may promote further applications of artificial intelligence-based laser fabrication in real industrial manufacturing.

4. Experimental Section

Experimental Setup

The ultrafast laser source was a Yb: YAG femtosecond laser system (Pharos 20, Light Conversion), with a central wavelength of 1030 nm, pulse duration of 256 fs and maximum repetition rate of 1 MHz. The focus length of laser processing system is 200 mm and the laser spot diameter is calculated as 50 μm. The polarization of laser beam can be controlled with a half-wave plate. The polarization state is maintained horizontal. Two galvo mirrors are combined to control the scanning of laser beam. The NVIDIA GeForce RTX 4060 is used for training and inference of neural network models.

Sample Preparation and Processing

The aluminum film is placed on a precise six-dimensional platform for a wide range moving of sample with a galvanometer to control the fast scanning of laser beam spot. The total travel of laser processing procedure is 100 mm and the maximum scanning speed can be set as 10 m/s.

Structure Characterization and Calculation of Chromaticity

Optical microscope images of aluminum sample and the corresponding color information are collected with the bright field mode of an optical microscope under the same observation condition to ensure consistency in color characterization. RGB labels were extracted from the relatively uniform areas of each microscope image to reduce edge effects and noise influence. The chromaticity coordinates in CIE 1931 chromaticity diagram are calculated based on the CIE 1931 standard from RGB values. The conversion process begins with normalizing the RGB values (0-255) to a floating-point range of [0, 1]. Subsequently, a standard sRGB gamma decoding (inverse gamma correction) is applied to linearize the RGB components. These linear RGB values are then transformed into the CIE 1931 XYZ tristimulus values using the standard sRGB-to-XYZ conversion matrix. The transformation is defined as:

$$\begin{pmatrix} X \\ Y \\ Z \end{pmatrix} = \begin{pmatrix} 0.4124 & 0.3576 & 0.1805 \\ 0.2126 & 0.7152 & 0.0722 \\ 0.0193 & 0.1192 & 0.9505 \end{pmatrix} \times \begin{pmatrix} R_{linear} \\ G_{linear} \\ B_{linear} \end{pmatrix} \tag{1}$$

Finally, the CIE(x,y) chromaticity coordinates are computed from the XYZ values using the standard formulas:

$$x = \frac{X}{X + Y + Z} \tag{2}$$

$$y = \frac{Y}{X + Y + Z} \tag{3}$$

Training and Validation Dataset

Experiments collected a dataset comprising 1,126 paired samples of laser processing parameters and their corresponding outcomes (texture images) with extracted RGB color information. The dataset was randomly partitioned into 900 training samples and 226 validation samples. Based on the experimental dataset, two supervised regression tasks were considered: (1) forward prediction from six process parameters (including two physical-driven parameters) to the three-channel RGB color; and (2) inverse regression from texture images to four key process parameters.

Calculation of physical parameters

The calculation formulas of beam overlap ratio (BOR) and average deposited energy (ADE) are defined as:

$$\text{Overlap Ratio} = \frac{\text{Repetition Rate}}{\text{Scanning Speed}} \tag{4}$$

$$\text{Average Power} = \text{Repetition Rate} \times \text{Pulse Energy} \tag{5}$$

Acknowledgements

This work is supported by the National Key R&D Program of China (2024YFB4609800), the National Natural Science Foundation of China (Grant No. 52575510), Deep Earth probe and Mineral Resources Exploration-National Science and Technology Major Project (Grant No. 2024ZD1000800，2024ZD1000805) and, 2022 Shenzhen `Pengcheng Peacock Plan' for providing the Special Talent A-class funding, specifically the Ma Zhaoyuan Research Start-up Fund (Grant No. Y01966114) and the joint research program between Tohoku University and Tsinghua University (No. 20253080015).

5. References

1 Geng, J., Xu, L., Yan, W., Shi, L. & Qiu, M. High-speed laser writing of structural colors for full-color inkless printing. *Nature Communications* **14**, 565, doi:10.1038/s41467-023-36275-9 (2023).

2 Lapidas, V. *et al.* Surface Coloring and Plasmonic Information Encryption at 50000 dpi Enabled by Direct Femtosecond Laser Printing. *Nano Letters* **24**, 12590-12596, doi:10.1021/acs.nanolett.4c03576 (2024).

3 Zhestkij, N. A. *et al.* Grayscale to Multicolor Laser Writing Inside a Label-Free Metal-Organic Frameworks. *Advanced Functional Materials* **34**, 2311235, doi:https://doi.org/10.1002/adfm.202311235 (2024).

4 Wang, Z. *et al.* Ultrafast Laser Inkless Full-Color Printing on Flexible and Thermolabile Substrates. *Advanced Optical Materials* **13**, 2402293, doi:https://doi.org/10.1002/adom.202402293 (2025).

5 Liping, S., Panpan, N., Qilin, J., Ji, Y. & Jiao, G. Ultrafast laser writing structural colors on TiAlN-TiN hybrid films. *Light: Advanced Manufacturing* **6**, 52-61, doi:10.37188/lam.2025.006 (2025).

6 Chen, H. *et al.* Advances in Photonic Crystal Research for Structural Color. *Advanced Materials Technologies* **10**, 2400865, doi:https://doi.org/10.1002/admt.202400865 (2025).

7 Wang, J. *et al.* Nanograting-Based Dynamic Structural Colors Using Heterogeneous Materials. *Nano-Micro Letters* **17**, 59, doi:10.1007/s40820-024-01554-7 (2024).

8 Zhu, X., Yan, W., Levy, U., Mortensen, N. A. & Kristensen, A. Resonant laser printing of structural colors on high-index dielectric metasurfaces. *Science Advances* **3**, e1602487, doi:10.1126/sciadv.1602487.

9 Chen, F. *et al.* Bio-inspired structural colors and their applications. *Chemical Communications* **57**, 13448-13464, doi:10.1039/D1CC04386B (2021).

10 Wan, W., Gao, J. & Yang, X. Full-Color Plasmonic Metasurface Holograms. *ACS Nano* **10**, 10671-10680, doi:10.1021/acsnano.6b05453 (2016).

11 Liu, Y. *et al.* Structural color three-dimensional printing by shrinking photonic crystals. *Nature Communications* **10**, 4340, doi:10.1038/s41467-019-12360-w (2019).

12 Li, J. *et al.* Dichroic Polarizing Metasurfaces for Color Control and Pseudo-Color Encoding. *IEEE Photonics Technology Letters* **33**, 77-80, doi:10.1109/LPT.2020.3045298 (2021).

13 Qiao, M., Yan, J. & Jiang, L. Direction Controllable Nano-Patterning of Titanium by Ultrafast Laser for Surface Coloring and Optical Encryption. *Advanced Optical Materials* **10**, 2101673, doi:https://doi.org/10.1002/adom.202101673 (2022).

14 Soltani-Kordshuli, F., Harris, N. & Zou, M. Tribological behavior of polydopamine/polytetrafluoroethylene coating on laser textured stainless steel with Hilbert curves. *Friction* **11**, 1307-1319, doi:10.1007/s40544-022-0671-0 (2023).

15 Boidi, G. *et al.* Fast laser surface texturing of spherical samples to improve the frictional performance of elasto-hydrodynamic lubricated contacts. *Friction* **9**, 1227-1241, doi:10.1007/s40544-020-0462-4 (2021).

16 Guo, H. *et al.* A review of ultrafast laser micro/nano fabrication: Material processing, surface/interface controlling, and devices fabrication. *Nano Research* **17**, 6212-6230, doi:10.1007/s12274-024-6644-z (2024).

17 Li, Y., Zhang, X., Zou, T., Mu, Q. & Yang, J. Vivid Structural Color Macropatterns Created by Flexible Nanopainting of Ultrafast Lasers. *ACS Applied Materials & Interfaces* **14**, 21758-21767, doi:10.1021/acsami.2c04542 (2022).

18 Luo, M. *et al.* Atomic-scale ultrafast laser processing of nanocrystal with plasmonic modulation for machine learning combined flexible sensor devices. *International Journal of Extreme Manufacturing* **8** (2025).

19 Li, B., Jiang, L., Li, X., Wang, Z. & Yi, P. Self-propelled Leidenfrost droplets on femtosecond-laser-induced surface with periodic hydrophobicity gradient. *International Journal of Extreme Manufacturing* **6**, doi:10.1088/2631-7990/ad18fb (2024).

20 Groussin, B. *et al.* Efficient Composite Colorization of Copper by Spatially Controlled Oxidation with Deep-UV Ultrafast Lasers. *Advanced Optical Materials* **12**, 2302071, doi:https://doi.org/10.1002/adom.202302071 (2024).

21 Xie, J. *et al.* Laser Induced Coffee-Ring Structure through Solid-Liquid Transition for Color Printing. *Small* **19**, 2205696, doi:https://doi.org/10.1002/smll.202205696 (2023).

22 Yao, J. *et al.* Selective appearance of several laser-induced periodic surface structure patterns on a

metal surface using structural colors produced by femtosecond laser pulses. *Applied Surface Science* **258**, 7625-7632, doi:https://doi.org/10.1016/j.apsusc.2012.04.105 (2012).

23 Hou, M. *et al.* Femtosecond Bessel laser beam induced concentric rings on SiC for circular symmetry wide-viewing angle structural color. *Optics & Laser Technology* **181**, 111813, doi:https://doi.org/10.1016/j.optlastec.2024.111813 (2025).

24 Liu, Y. *et al.* Single-Pixel-Adjustable Structural Color Fabricated Using a Spatially Modulated Femtosecond Laser. *ACS Applied Materials & Interfaces* **15**, 49805-49813, doi:10.1021/acsami.3c10666 (2023).

25 Vorobyev, A. Y. & Guo, C. Direct femtosecond laser surface nano/microstructuring and its applications. *Laser & Photonics Reviews* **7**, 385-407, doi:https://doi.org/10.1002/lpor.201200017 (2013).

26 Hwang, T. Y. *et al.* Deep learning-based optical authentication using the structural coloration of metals with femtosecond laser-induced periodic surface structures. *Opt. Express* **31**, 1776-1786, doi:10.1364/OE.478670 (2023).

27 Jhang, Y.-J. *et al.* PD-TNN: Physics-Driven Tandem Neural Network for Color Prediction in Laser-Induced Thin Films. *ACS Photonics* **12**, 4296-4304, doi:10.1021/acsphotonics.5c00563 (2025).

28 Roberts, N. B. & Keshavarz Hedayati, M. A deep learning approach to the forward prediction and inverse design of plasmonic metasurface structural color. *Applied Physics Letters* **119**, 061101, doi:10.1063/5.0055733 (2021).

29 Ma, H. *et al.* Predicting Laser-Induced Colors of Random Plasmonic Metasurfaces and Optimizing Image Multiplexing Using Deep Learning. *ACS Nano* **16**, 9410-9419, doi:10.1021/acsnano.2c02235 (2022).

30 Zhao, H. *et al.* Parametric analysis and a predictive model for color difference during laser-induced coloration on titanium. *Opt. Express* **30**, 33538-33553, doi:10.1364/OE.468964 (2022).

31 Buchnev, O. *et al.* Deep-Learning-Assisted Focused Ion Beam Nanofabrication. *Nano Letters* **22**,

2734-2739, doi:10.1021/acs.nanolett.1c04604 (2022).

32 Raissi, M., Perdikaris, P. & Karniadakis, G. E. Physics-informed neural networks: A deep learning framework for solving forward and inverse problems involving nonlinear partial differential equations. *Journal of Computational Physics* **378**, 686-707, doi:https://doi.org/10.1016/j.jcp.2018.10.045 (2019).

33 Peng, S. *et al.* Prediction of 3D temperature field through single 2D temperature data based on transfer learning-based PINN model in laser-based directed energy deposition. *Journal of Manufacturing Processes* **138**, 140-156, doi:https://doi.org/10.1016/j.jmapro.2025.02.015 (2025).

34 Shimahara, K., Tani, S., Sakurai, H. & Kobayashi, Y. A deep learning-based predictive simulator for the optimization of ultrashort pulse laser drilling. *Communications Engineering* **2**, 1, doi:10.1038/s44172-022-00048-x (2023).

35 Rohman, M. N., Ho, J.-R., Tung, P.-C., Tsui, H.-P. & Lin, C.-K. Prediction and optimization of geometrical quality for pulsed laser cutting of non-oriented electrical steel sheet. *Optics & Laser Technology* **149**, 107847, doi:https://doi.org/10.1016/j.optlastec.2022.107847 (2022).

36 Shugaev, M. V. *et al.* Fundamentals of ultrafast laser–material interaction. *MRS Bulletin* **41**, 960-968, doi:10.1557/mrs.2016.274 (2016).

Electronic Supplementary Material

Prediction and inverse design for ultrafast laser colorization on aluminum via color-morphology coupled neural network

Xianghong Xu[1,§], Jiaqun Li[2,3,§], Junjie Li[4], Haoze Han[2,3], Rui Han[2,3], Weiqing Li[1,], Zhaoyuan Ma[4], Yuichi Kozawa[5], and Jianfeng Yan[2,3,*]*

[1]School of Engineering and Technology, China University of Geosciences (Beijing), Beijing 100083, China

[2]Department of Mechanical Engineering, Tsinghua University, Beijing 100084, China

[3]State Key Laboratory of Tribology in Advanced Equipment, Tsinghua University, Beijing 100084, China

[4]School of Automation and Intelligent Manufacturing, Southern University of Science and Technology, Shenzhen 518055, China

[5]Institute of Multidisciplinary Research for Advanced Materials, Tohoku University, 2-1-1 Katahira, Aoba-Ku, Sendai 980-8577, Japan

[§]Xianghong Xu and Jiaqun Li contributed equally to this work.

Address correspondence to Weiqing Li, liweiqing@cugb.edu.cn; Jianfeng Yan, yanjianfeng@tsinghua.edu.cn

Supporting information to https://doi.org/10.26599/NR.2026.94908535

Model Training and Validation

Two supervised regression tasks were considered: (1) forward prediction from six process parameters (including two physical-driven parameters) to the three-channel RGB color; and (2) inverse regression from texture images to four key process parameters.

The forward model adopted a physics-guided multilayer perceptron (PG-MLP) for the prediction task. By incorporating physically meaningful guidance, PG-MLP improves data efficiency and generalization while maintaining a compact architecture suitable for the training set size (~900), thereby mitigating overfitting risk; the predictive performance meets application needs empirically. For the inverse task, mapping from RGB alone to process parameters constitutes an underdetermined low-to-high-dimensional inference with information loss; our experiments confirmed that MLPs trained solely on RGB inputs fail to learn a reliable mapping. We therefore employed a convolutional architecture, EfficientNet-B0, with images as inputs so that the model can jointly exploit color and texture statistics to enhance inversion accuracy and robustness. All continuous variables were standardized to a zero mean and unit variance. In the forward task, both the input process parameters and the RGB outputs were standardized; in the inverse task, the four target process parameters were standardized. Images were normalized following standard vision practice; The RGB optical images were resized to 224 × 224 pixels and converted to tensors. All images were normalized using standard ImageNet parameters (mean = [0.485, 0.456, 0.406], std = [0.229, 0.224, 0.225]). In order to promote generalization, random horizontal flipping (p=0.3) and random vertical flipping (p=0.2) were applied during training for data augmentation. To maintain intrinsic color distributions and texture features, augmentation techniques that affect color and structure information were excluded.

Both tasks were optimized with Adam. The forward model used a relatively higher learning rate suitable for shallow tabular networks; the inverse model adopted a lower learning rate with weight decay for stable fine-tuning. A Reduce-on-Plateau scheduler, driven by validation R^2, adaptively reduced the learning rate upon performance stagnation, and early stopping was used to curb overfitting. For the forward PG-MLP, we used ReLU and light dropout, a learning rate of 10^{-4}, a batch size of around 64, and a sufficiently large epoch cap to allow convergence; the best model was selected by validation R^2. For the inverse EfficientNet-B0, we fine-tuned the whole network with a learning rate on the order of 10^{-5}, weight decay for regularization, and gradient clipping for stability; the loss combined mean squared error and mean absolute error as $0.8\times \mathrm{MSE} + 0.2\times \mathrm{L1}$ with equal weights across parameters to balance convergence speed and robustness.

Performance was assessed using the coefficient of determination (R^2), root-mean-square error (RMSE), and Pearson correlation; for multi-output targets, we reported both per-channel (or per-parameter) and averaged correlations. In addition to standardized-space metrics, predictions and references were de-standardized for the forward task to report RMSE in the original RGB space for physical interpretability. Throughout training, we logged losses, R^2, RMSE, Pearson correlations, and learning-rate dynamics. To support reproducibility and comparative analysis, we selected the best model based on validation R^2, training curves, and prediction−ground-truth scatter plots. For the inverse design results of laser parameters, the Pearson correlation coefficients are 0.3071 for pulse energy, 0.5057 for scanning speed and 0.8427 for average power.

Inverse design results without morphological information

The training results of inverse model using only RGB input are displayed in **Figure S1.** These scatter plots show weak correspondence between the real values and inverse-deigned parameters. Data points not closely aligning with the 45-degree line of perfect agreement. These results demonstrate that the improvement performance can be achieved by incorporating morphological information into the network model.

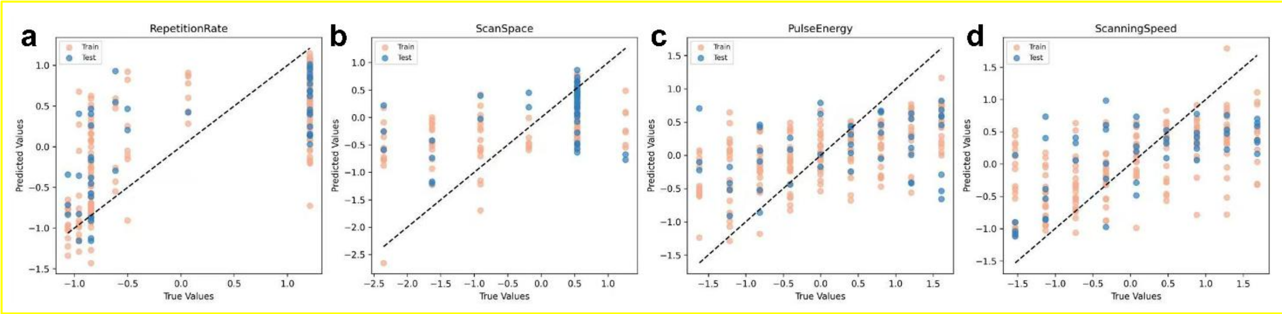

Figure S1. Scatter plots for the demonstration of difference between the inverse-deigned parameters using only RGB input and real values of the test dataset.

Training results with different models

The training results of different models are displayed in **Tabel S1**. When the extra physical parameters like the scanning overlap and average power are introduced into the training model, the Pearson correlation coefficients of RGB value in network are promoted obviously. Meanwhile, the R^2 of training model is raised from 0.74 to 0.82.

Table S1. The comparison of training results with different models

Pearson correlation coefficients	Model without Extra Physical parameters	Model with Extra Physical parameters
Red (R)	0.8865	0.9222
Green (G)	0.8742	0.9156
Blue (B)	0.8512	0.8908
Average	0.8706	0.9095

Besides of the RGB values, the Lab values of structural color are also considered and compared in the model training. The conversion from RGB color values to LAB color values is based on CIE chromaticity as an intermediate medium value. The training results of Lab values are shown in **Table S2**. Considering the training results of RGB values is better than that of Lab values, the RGB values are utilized in the final training models.

Table S2. The comparison of training results using the Lab values

Pearson correlation coefficients	Model without Extra Physical parameters	Model with Extra Physical parameters
Luminosity (L)	0.8642	0.9147
a	0.5914	0.6900
b	0.7846	0.8835
Average	0.7467	0.8294